arXiv:1408.4078v2 [cond-mat.str-el] 9 Dec 2014

Unquenched e_g^1 orbital moment in the Mott-insulating antiferromagnet $KOsO_4$

Young-Joon Song[1], Kyo-Hoon Ahn[1], Kwan-Woo Lee[1,2,*] and Warren E. Pickett[3†]
[1] *Department of Applied Physics, Graduate School, Korea University, Sejong 339-700, Korea*
[2] *Department of Display and Semiconductor Physics, Korea University, Sejong 339-700, Korea*
[3] *Department of Physics, University of California, Davis, California 95616, USA*
(Dated: December 10, 2014)

Applying the correlated electronic structure method based on density functional theory plus the Hubbard U interaction, we have investigated the tetragonal scheelite structure Mott insulator $KOsO_4$, whose e_g^1 configuration should be affected only slightly by spin-orbit couping (SOC). The method reproduces the observed antiferromagnetic Mott insulating state, populating the Os d_{z^2} majority orbital. The quarter-filled e_g manifold is characterized by a symmetry breaking due to the tetragonal structure, and the Os ion shows a crystal field splitting $\Delta_{\rm cf} = 1.7$ eV from the t_{2g} complex, which is relatively small considering the high formal oxidation state Os^{7+}. The small magnetocrystalline anisotropy before including correlation (i.e., in the metallic state) is increased by more than an order of magnitude in the Mott-insulating state, a result of a strong interplay between large SOC and a strong correlation. In contrast to conventional wisdom that the e_g complex will not support orbital magnetism, we find that for the easy axis [100] direction the substantial Os orbital moment $M_L \approx -0.2\mu_B$ compensates half of the Os spin moment $M_S = 0.4\mu_B$. The origin of the orbital moment is analyzed and understood in terms of additional spin-orbital lowering of symmetry, and beyond that due to structural distortion, for magnetization along [100]. Further interpretation is assisted by analysis of the spin density and the Wannier function with SOC included.

PACS numbers: 71.20.Be, 71.27.+a, 71.30.+h

I. INTRODUCTION

In condensed matter, especially when containing heavy ions, spin-orbit coupling (SOC) leads to phenomena that are lacking without SOC. Examples of recent interest include the original topological insulators,[1] behavior arising from the Rashba effect, unconventional metal-insulating transitions, compensating spin and orbital moments,[2,3] and the magnetocrystalline anisotropy (MCA) that is so important in spintronics applications. Whereas SOC within a t_{2g} manifold in a MO_6 octahedron (M = transition metal) has a long history[4–6] and has been intensively discussed recently in several specific contexts,[2,7–11] corresponding effects in an e_g manifold have rarely been considered due to the conventional wisdom that the e_g subshell ensures a perfectly quenched orbital moment. From this viewpoint, heavy transition metal oxides containing MO_4 tetrahedra are of great interest, since crystal field splitting leads to partially filled orbitals in the e_g manifold.

About a century ago, monoclinic crystals of two toxic, volatile materials, OsO_4 and RuO_4, were synthesized. These are presumably textbook band insulators, albeit with remarkably high (8+) formal charges. Although existing data on these crystals are limited, the effects of SOC have been investigated from a chemical viewpoint since the 1990's[12–14] and have been generally found to be minor. In 1985, heptavalent $AOsO_4$ (A = alkali metal) compounds were synthesized by Levason *et al.*, who determined they formed in the tetragonal scheelite crystal structure.[15] $KOsO_4$ has been often synthesized from a mixture of KO_2 and Os metal as a precursor for preparation of the superconductor KOs_2O_6,[16] but further investigations of its physical properties are still lacking. $KOsO_4$ seems to be insulating, though detailed resistivity data are not yet available.[17,18]

Recently, Yamaura and collaborators determined the crystal structure parameters and measured the susceptibility and specific heat.[18] The Curie-Weiss moment is $\mu_{\rm eff} = 1.44\mu_B$, 20% reduced from the spin-only moment, and the Néel temperature is $T_N = 37$ K. These authors suggested that magnetic frustration in this distorted diamond lattice may be necessary to account for observations. However, the conventional ratio of Curie-Weiss to ordering temperatures $|\theta_{CW}|/T_N \approx 1.8$ is small (i.e., there is little frustration in the bipartite Os sublattice) so other factors must be considered.

In this paper we study the electronic structure of $KOsO_4$, with special attention given to the interplay between strong correlation and SOC. The small ligand field splitting of the e_g orbitals due to distortion of the OsO_4 tetrahedron plays an important role in determining the occupied orbital in the Mott-insulating state, and may become active in effects arising from SOC as well. A modest t_{2g}-e_g crystal field splitting ($\Delta_{\rm cf} = 1.7$ eV) and large SOC strength ($\sim$0.3 eV) bring in another effect of crystallinity that impacts the effects of SOC. This splitting is especially small considering that in another Os^{7+} compound, the double perovskite Ba_2NaOsO_6, $\Delta_{\rm cf} = 6$ eV is extremely large.[2] Results are analyzed in terms of magnetization densities, Wannier functions, and spin-orbital occupation numbers. Symmetry reduction of the electronic state due to SOC when the spin lies in the [100] direction is found to have a great consequence: A population imbalance of the $m_l = \pm 2$ orbitals leads to an unexpectedly large orbital moment, as discussed in Sec. V.

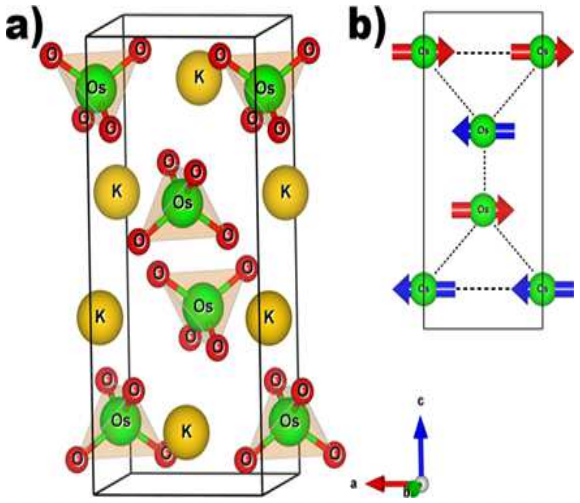

FIG. 1: (Color online) (a) Scheelite-type crystal structure of $KOsO_4$. (b) G-type antiferromagnetic (AFM) spin ordering, which is the ground state in LSDA+U+SOC calculations. The arrows indicate the calculated directions of spins (easy axis).

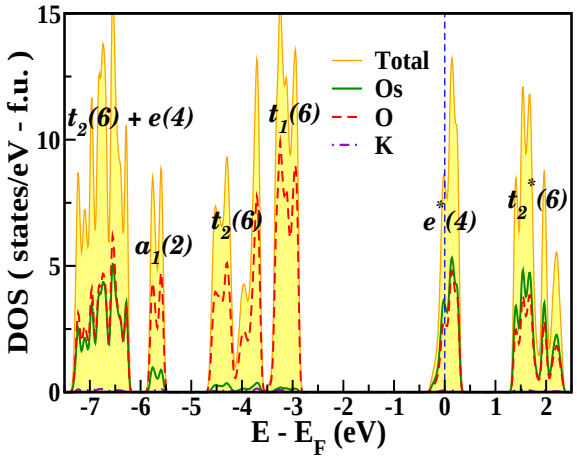

FIG. 2: (Color online) LDA total and atom-projected densities of states (DOS) of nonmagnetic $KOsO_4$ in the regimes of Os $5d$ and O $2p$ orbitals. The symbols, which are displayed in each manifold, represent the molecular orbitals of the OsO_4 tetrahedron, following the notations of Ref. [25]. The values in parentheses indicate the number of bands in each manifold. The symbol $*$ denotes the antibonding state. The DOS $N(E_F)$ at the Fermi energy E_F, which is set to zero, is 4.18 states/eV f.u. spin.

II. STRUCTURE AND CALCULATION METHODS

$KOsO_4$ crystallizes in the scheelitelike structure (space group: $I4_1/a$, No. 88), shown in Fig. 1. In this tetragonal structure with two formula units (f.u.) per primitive cell, the lattice parameters are $a = 5.652$ Å and $c = 12.664$ Å,[?] leading to a ratio of $c/\sqrt{2}a = 1.58$. The Os sublattice forms a substantially elongated diamond sublattice; this $c/\sqrt{2}a$ ratio is unity for the cubic diamond lattice. The K and Os atoms sit at the $4b$ sites $(0,\frac{1}{4},\frac{5}{8})$ and $4a$ sites $(0,\frac{1}{4},\frac{1}{8})$, respectively. The O atoms lie on the $16f$ sites (0.1320,0.0160,0.2028). In the OsO_4 tetrahedron, all Os-O bond lengths are 1.81 Å, and the O-Os-O bond angles are either 114° or 107°, compared to 109.5° for a regular tetrahedron. A similar distortion is observed in the band insulator OsO_4,[19] while both RuO_4 and $KRuO_4$ have nearly ideal tetrahedra.[20,21] This difference suggests that the distortion is due to a chemical difference between Os and Ru ions.

Our calculations were carried out with the local (spin) density approximation [L(S)DA] and its extensions, as implemented in the accurate all-electron full-potential code WIEN2K.[22] Since we are interested in a possible competition between large SOC and strong correlation effects in magnetic systems, we compare all of the LDA, LSDA, LSDA+SOC, LSDA+U, and LSDA+U+SOC approaches. An effective on-site Coulomb repulsion U was used for the LDA+U calculations; since Os^{7+} is a d^1 ion which is not occupied by more than one electron, the Hund's rule coupling J between two electrons of the same spin was set to zero. To analyze the partially filled Os complex, the Wannier function approach implemented in FPLO and WIEN2K has been used.[23,24] Calculations of the Wannier function including SOC are available only in the latter. In WIEN2K, the following muffin-tin radii are adopted: 2.02 for Os, 1.4 for O, and 2.2 for K (in units of a.u.). The extent of the basis was determined by $R_{\rm mt}K_{\rm max} = 7$. The Brillouin zone was sampled with a sufficiently dense k mesh (for an insulator) of $13\times13\times6$.

III. THE UNDERLYING ELECTRONIC STRUCTURE

Figure 2 displays the LDA total and atom-projected densities of states (DOSs), which demonstrates a strong p-d hybridization not only in the most relevant Os e_g bands (denoted as the molecular e^* orbitals) but also in more tightly bound oxygen orbitals around –7 eV. This hybridization of the transition metal d character into O $2p$ bands is common but is not particularly relevant and is little discussed. The narrow bands reflect moderately banding molecular orbitals. Some nearly pure oxygen bands lie in the –6 to –3 eV range. The t_2^* bands centered around 2 eV are a mixture of Os t_{2g}, and all O $2p$ orbitals, while the e^* set is a mixture of e_g and mostly p_π.

Before considering the complications of spin polarization, correlation effects, and SOC, we consider the basic underlying features of the electronic structure. Supposing formal charges of K^+, Os^{7+}, and O^{2-} ions, the crystal field e_g–t_{2g} splitting is expected to be 0.8 eV, about half of the calculated splitting $\Delta_{\rm cf} = 1.7$ eV, which is the full ligand field splitting.

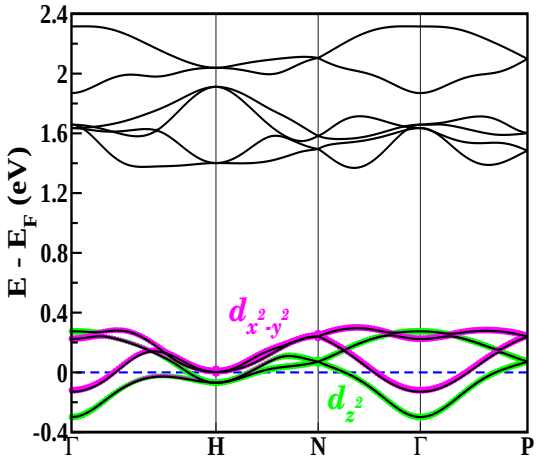

FIG. 3: (Color online) LDA Os 5d band structure of nonmagnetic $KOsO_4$, showing an e_g–t_{2g} crystal field splitting of ∼1.8 eV. The partially filled e_g bands, which are colored with the corresponding Wannier orbitals, lie on the range of –0.3 to 0.3 eV. In units of $(\pi/a,\pi/a,\pi/c)$, the symmetry points shown are $H = (100)$, $N = (\frac{1}{2}\frac{1}{2}0)$, and $P = (\frac{1}{2}\frac{1}{2}\frac{1}{2})$.

The LDA nonmagnetic band structure in the Os 5d band region (ten bands due to 2 f.u. per primitive cell) is displayed in Fig. 3. The distortion of the OsO_4 tetrahedron leads to the crystal field splitting of d_{xy} above the degenerate pair $\{d_{xz},d_{yz}\}$, as is evident in Fig. 3. Notably, the isolated partially filled e_g manifold can be fit well using an effective two-band model with three nearest neighbor hopping parameters. The hopping parameters corresponding to the corresponding Wannier functions are

$$\begin{aligned} t_1 = &\quad \langle d_{x^2-y^2} \mid \hat{H} \mid d_{x^2-y^2}\rangle &&= 43 \text{ meV}, \\ t_2 = &\quad \langle d_{z^2} \mid \hat{H} \mid d_{z^2}\rangle &&= 56 \text{ meV}, \\ t' = &\quad \langle d_{z^2} \mid \hat{H} \mid d_{x^2-y^2}\rangle &&= 7 \text{ meV}. \end{aligned} \quad (1)$$

The site energies are 59 meV for d_{z^2} and 143 meV for $d_{x^2-y^2}$ relative to E_F. It is this ligand field splitting of 84 meV that determines that the d_{z^2} becomes occupied in the Mott-insulating phase (below). As expected from the small value of t', each of the $d_{x^2-y^2}$ and d_{z^2} bands can be fit nearly as well along symmetry lines using two independent single band models. A noticeable mixing between the two bands only occurs along the Γ-H line. The superexchange coupling parameter is determined from $J = t^2/U \sim 2$ meV, using $U = 2$ eV (see below). The magnitude of this exchange coupling is similar to the ordering temperature $k_B T_N \approx 3$ meV.

IV. EFFECTS OF CORRELATION AND SOC

A primary emphasis in our study of this system is to assess the interplay in an e_g system between strong correlations, which prefer full occupation of certain orbitals and usually increase spin polarization, and SOC, which mixes spin orbitals and complicates all aspects of the electronic structure while inducing the orbital moment and magnetocrystalline anisotropy (MCA). It was mentioned above that including correlation effects in the LSDA+U method leads to preferred occupation of the d_{z^2} orbital, which has 84 meV lower on-site (crystal field) energy than $d_{x^2-y^2}$ due to the distortion of the OsO_4 tetrahedron. The band structures including the lower part of the t_{2g} complex, and the DOS of the e_g bands alone for the energetically preferred AFM state, are displayed in Figs. 4 and 5, respectively. These figures have been constructed to allow identification of the individual effects of U and SOC.

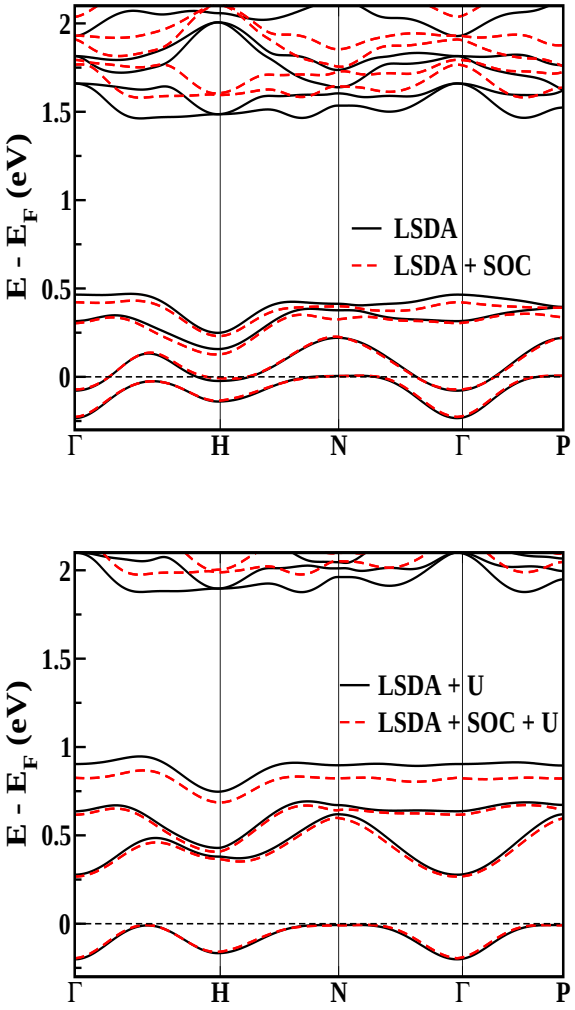

FIG. 4: (Color online) AFM band structures of (top) LSDA without and with SOC, and (bottom) LSDA+U without and with SOC, for $U = 2$ eV. In the insulating state, the occupied state is mainly d_{z^2}.

Before proceeding with a description of the full electronic structure and then the spin density itself, we re-

TABLE I: Effect of correlation U on the relative energies ΔE (in units of meV/f.u.) and Os orbital moments M_L (in units of μ_B) for each of four spin quantization directions and for FM and AFM alignments. M_L of Os is antialigned to the spin moment of Os, which is $\sim 0.4\mu_B$ for the insulating states. The spin moments contributed by O ions are 0.24 – $0.32\mu_B$/4O in LSDA+SOC, increasing to $\sim 0.4\mu_B$/4O for LSDA+SOC+U. $U = 2$ eV was used for LSDA+SOC+U calculations.

		AFM				FM			
		[100]	[001]	[110]	[111]	[100]	[001]	[110]	[111]
LSDA+SOC	ΔE	0	4.6	2.3	3.7	1.9	3.9	1.8	3.4
LSDA+U+SOC	ΔE	0	14.4	3.0	10.6	19.3	28.7	19.8	26.2
LSDA+SOC	M_L	–0.134	–0.014	–0.136	–0.052	–0.135	–0.048	–0.135	–0.073
LSDA+U+SOC	M_L	–0.184	0.007	–0.183	–0.053	–0.176	0.006	–0.172	–0.055

view the energy differences arising from the various interactions.

A. Magnetic Energy Differences

As expected from the peak at E_F in the DOS (see Fig. 2) and the well known Stoner instability, ferromagnetism (FM) is energetically favored over the nonmagnetic state, by 26 meV/f.u. Our fixed spin moment calculations of the interacting susceptibility[26] lead to $IN(E_F) = 1.60$, well above the Stoner instability criterion of unity, and $N(E_F) = 4.09$ states/eV f.u. spin gives the Stoner parameter $I = 0.39$ eV, similar to the value obtained[2] for Ba_2NaOsO_6. Within metallic LSDA where exchange coupling might be considered to be some mixture of double exchange, Ruderman-Kittel-Kasuya-Yosida (RKKY), and superexchange, the FM ground state lies 5.5 meV/f.u. below the observed AFM state.

To assess the effects of SOC before including correlation corrections, we display MCA energies with LSDA+SOC with several spin orientations in Table I. [100] is the AFM easy axis, however, all spin orientations differ little in energy compared to the larger differences when all interactions are included (see below), so the magnetic anisotropy is predicted to be small at this level of theory. This tentative conclusion, before including correlation, is consistent with conventional wisdom that SOC has little effect in e_g systems.

After including correlation with $U = 2$ eV, the AFM Mott-insulating state is obtained (discussed below) as the ground state, by 19 meV over FM alignment. This favoring of antiferromagnetism over ferromagnetism is common when applying the LDA+U functional in transition metal oxides. For bipartite AFM (alternating) alignment compared to FM alignment, the AFM magnetic coupling is $J \approx 4.8$ meV ≈ 56 K, consistent in magnitude with the experimental ordering temperature $T_N = 37$ K.

Other aspects of the interplay between strong SOC and strong correlation are apparent in Table I. Most notable in the energetics is that strong correlation effects (i.e., including U) greatly enhance the MCA: Energy differences between different directions of the spin are more than an order of magnitude larger. This is more surprising when one recalls that SOC effects (which provide the MCA) are often supposed to be negligible in e_g subshells. Including both large U and SOC, the [100] direction is now very clearly determined as the easy axis.

B. LSDA+SOC+U leads to a Mott-insulating state

The lowest and highest bands (Fig. 4) in the e_g manifold extending over the regime of –0.25 to + 0.5 eV are the Os spin-up and spin-down d_{z^2} bands, respectively. In the quarter-filled e_g manifold, the d_{z^2}-$d_{x^2-y^2}$ degeneracy lifting is 0.2 eV, i.e., the e_g degeneracy is already split (presumably self-consistently by occupation of the d_{z^2} orbital and the resulting Jahn-Teller distortion). Applying the on-site Coulomb repulsion U starting from small values leads to a metal-insulator transition (MIT) (gap opening) at a critical value $U_c \approx 1.2$ eV, which is near the bottom of the range of expected values for Os. As shown in the bottom panel of Fig. 4 for $U = 2$ eV and spin along the [100] direction, the top of the occupied band has a flat region around the N point, giving rise to a one-dimension-like peak and sharp discontinuity in the DOS at the top of the band, evident in Fig. 5. Other band maxima at P and midway between Γ and N are (somewhat accidentally) degenerate with the flat band at N. The occupied bandwidth is 0.2 eV. As shown by the red dashed lines in the band structure of Fig. 4, inclusion of SOC a has negligible effect on the occupied state (position and dispersion) but lowers the uppermost e_g band (primarily minority spin) by 0.15 eV. This shift corresponds to a small decrease in the exchange splitting of the unoccupied e_g orbital.

C. Effects of SOC on spin and orbital moments

In the following text and in Table I we quote atomic moments from contributions within the inscribed spheres, which are somewhat smaller than the full value. We remind that the occupied "d_{z^2}" orbital that is occupied before including SOC is strongly hybridized with $2p$ orbitals of the surrounding O ions, so the spin magnetization of $1\mu_B$ is distributed over oxygen as well as Os. The

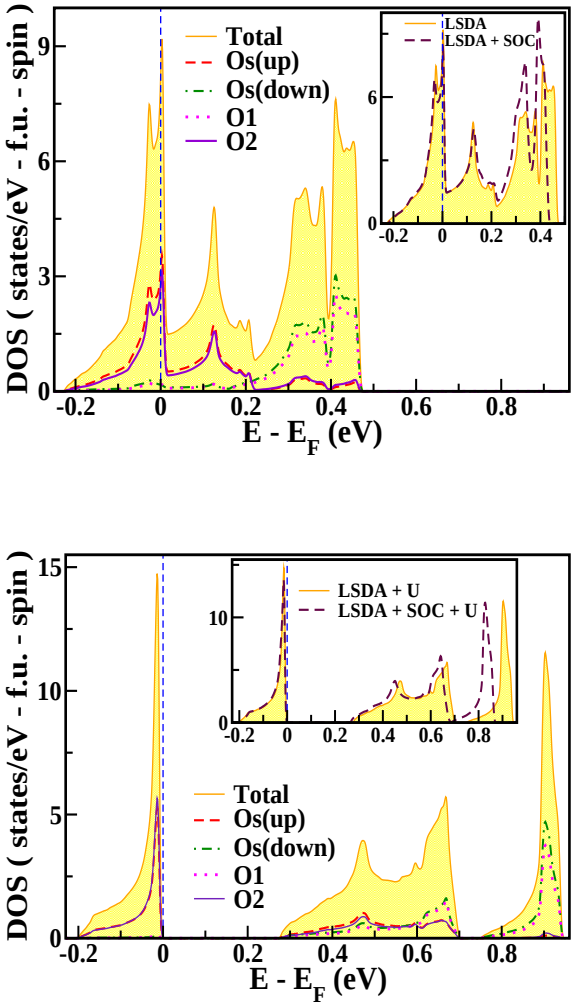

FIG. 5: (Color online) AFM densities of states of (top) LSDA and (bottom) LSDA+U at $U = 2$ eV, with atomic contributions differentiated. *Inset*: Comparison of DOS with the case including SOC, near E_F. In the metallic $U = 0$ state, the exchange splitting in the e_g manifold is 0.4 eV. In the insulating state, in terms of the spin-up Os, the plots contain the filled spin up d_{z^2}, the unfilled $d_{x^2-y^2}$, and the unfilled spin down d_{z^2} bands, from the lower energy. In LSDA, $N(E_F) \approx 4$ states/eV spin f.u., but lies on a very sharp edge. Inclusion of SOC reduces $N(E_F)$ by 7%.

moment values should be considered in conjunction with the spin density isosurfaces pictured in Fig. 6.

For all spin orientations we have determined that the Os spin moment is $M_S \approx 0.4\mu_B$. This value is almost independent of U in the range 0–5 eV that we have studied. The O net spin $M_S = 0.07\mu_B$/O aligns parallel to that of the nearest neighbor Os. The sum of the full atom moments must be unity, so atomic values are around $0.5\mu_B$ and $0.12\mu_B$ for Os and O, respectively, versus the atomic sphere values just quoted. Including SOC reduces the Os spin moment by 10%, transferring the difference to

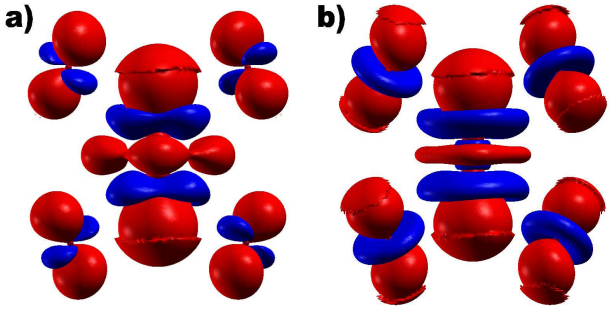

FIG. 6: (Color online) Isosurface plots at 0.042 $e/\text{Å}^3$ of spin densities for (a) metallic ($U = 0$) and (b) insulating AFM ($U = 2$ eV) $KOsO_4$, when including SOC. Os at the center is surrounded by four O ions. Red indicates majority spin, and blue denotes minority. The insulating density in (b) reflects the circular shape around both Os and O that provides the orbital moment.

neighboring O M_S due to rehybridization. Nonzero M_L must arise from mixing in of t_{2g} character, as we discuss in Sec. V. For [100] and [110] spin directions, increasing U increases $|M_L|$ from $\sim 1/3 M_S$ at $U = 0$ to $1/2 M_S$ at $U = 2$ eV. For [001] spin orientation M_L is essentially vanishing for any value of U (Table I).

D. Behavior of the spin density

The spin density isosurface plots displayed in Fig. 6 for metallic ($U = 0$) and AFM insulating ($U = 2$ eV) phases are instructive. Even in the metallic, uncorrelated case both positive and negative lobes of spin density appear on both Os and O ions, indicating more complexity than strong (but typically simple) p-d hybridization. Since in this limit the lower Hubbard band is fully polarized (only spin-up states), the negative polarization arises from polarization within the filled nominally O $2p$ bands at lower energy.

The net spin of O lies in $2p$ orbitals whose orientation reflects a π antibonding character with Os d_{xz}, d_{yz} orbitals. A small negative spin density is induced in a linear combination of the p_x, p_y orbitals, in the local coordinate system. As expected, the Os spin lies mainly in the d_{z^2} orbital, with some admixture of $d_{x^2-y^2}$ accounting for the square versus circular symmetry of the spin density in the equatorial plane of Os. A small but clear admixture of d_{yz} and d_{xz} character appears as a negative spin density (blue), and this contribution is necessary to provide the Os orbital moment.

In the correlated ($U = 2$ eV) insulating state, Os still has mainly a d_{z^2} character for spin up. However, the circular symmetry indicating d_{yz}-id_{xz} character for spin down shows up much more clearly. Unexpectedly, this same development of p_x-ip_y (in an appropriate local frame) shows up on the O ions in the spin-down re-

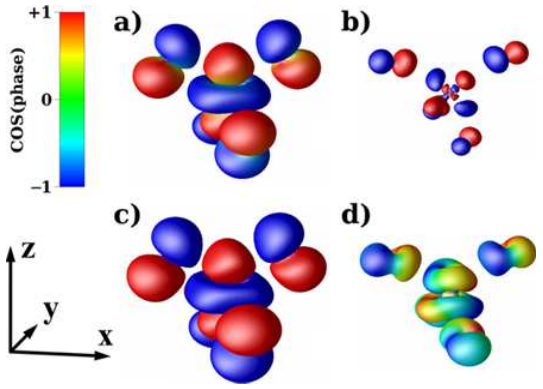

FIG. 7: (Color online) Isosurface plots of the Wannier function density $|W_\sigma(r)|^2$ of the occupied band in AFM insulating $KOsO_4$(LSDA+U+SOC with $U = 2$ eV), for the majority $\sigma = |\uparrow\rangle$ and minority $\sigma = |\downarrow\rangle$ spins separately. The surfaces are colored with the cosine of the phase of each component (real positive, red; real negative, blue; imaginary. green), as described in color legend bar. (a), (b) Spin in the [100] direction; (c), (d) spin in the [001] direction. (a) and (c) are for the majority spin, shown at isovalue = 2 a.u. (b) and (d) are for the minority spin, shown at the smaller isovalue of 0.3 a.u. While the minority spin component is small, its directional dependence is evident, with a much larger imaginary part for [001].

gion, while the spin-up, local p_x character is nearly undisturbed.

To generate the complex-valued, mixed-spin Wannier function $W(r)$ of the occupied band, we projected from $|\frac{5}{2}, \frac{1}{2}\rangle$ and $|\frac{3}{2}, \frac{1}{2}\rangle$ as a trial function in the WIEN2WANNIER package. Figure 7 presents isosurface plots of $|W(r)|^2$ for each of the two components of spin. The spin-down part is much smaller than the spin-up part, as indicated separately by the spin moment which remains close to $1\mu_B$/f.u. Consistent with Eqs. (2) and (3) below, the spin-down parts are d_{xz}-like in the [100] direction and d_{xz}-id_{yz}-like in the [001] direction. The spin-up parts are d_{z^2}-like in both directions, but have a squarish negative lobe rather than a circular shape. The complex character of the spin-up part in the [100] direction is visible only around the neck of the positive lobe, since the imaginary part is small. However, this complex character leads to a symmetry breaking between $m_l = \pm 2$ orbitals, as will be discussed below. The spin-up part in the [001] direction is purely real.

V. ANALYSIS OF SPIN-ORBIT COUPLING IN THE e_g^1 CASE

Now we address the effects of SOC, especially the appearance of a surprisingly large orbital moment in an e_g subshell which should not produce an orbital moment, through analysis of the occupation matrices and the associated Wannier function. SOC effects in the e_g channel tend to be relegated to the background because e_g contains only orbital $m_l = 0$ and $m_l = \pm 2$ d orbitals, which are not coupled by the electron spin $s = \frac{1}{2}$. Note, however, that this is strictly true only in the spherical (isolated ion) limit and for orbital moments along the axis of quantization, i.e., the direction of the spin. Indeed, we find negligible orbital moments for spin along [001]. Crystalline effects break this orbital-moment killing symmetry.

First, in $KOsO_4$, the crystal field splitting $\Delta_{\rm cf} = 1.7$ eV is slightly larger than the SOC strength, so virtual inclusion of t_{2g} orbitals may be involved. Second, the OsO_4 tetrahedron is distorted, breaking the twofold e_g symmetry, which is related to the Mott-insulating behavior: occupation of a single e_g orbital and the accompanying Jahn-Teller distortion. Finally, the higher symmetry crystalline $\hat{z}$ axis is not the easy axis, so additional complexities arise. The focus begins with the d_{z^2} orbital that is occupied before SOC is included, with a slight admixture of other $5d$ orbitals due to structural symmetry breaking and hopping.

Spin along [001]. Applying $\vec{L} \cdot \vec{S}$ to the spin-up d_{z^2} orbital leads to

$$\vec{L} \cdot \vec{S}|d_{z^2}\rangle|\uparrow\rangle_z \propto -(|d_{xz}\rangle + i|d_{yz}\rangle)|\downarrow\rangle_z, \qquad (2)$$

which are nominally unoccupied orbitals. Indeed, we calculate negligible M_L for this orientation, reflecting negligible intermixing of $d_{xz} \pm id_{yz}$ orbitals across the crystal field gap $\Delta_{\rm cf}$. The main occupation amplitudes (eigenvectors of the occupation matrix) are (in $|m_l, m_S\rangle$ notation), 0.96 for $|0, \uparrow\rangle$ and a down-spin amplitude of –0.21 for $|+1, \downarrow\rangle$ (thus decreasing the spin moment by 4%).

Spin along [100]. For in-plane [100] spin orientation SOC leads to the common picture

$$\vec{L} \cdot \vec{S}|d_{z^2}\rangle|\uparrow\rangle_x \propto -i|d_{yz}\rangle|\uparrow\rangle_x - |d_{xz}\rangle|\downarrow\rangle_x. \qquad (3)$$

Another way to approach the emergence of an orbital moment is to note that when the d_{z^2} orbital is expressed in local coordinate system X, Y, Z, with Z directed along [100], it is a linear combination of d_{Z^2} and $d_{X^2-Y^2}$ orbitals (i.e., the e_g orbitals). Breaking of symmetries may induce an asymmetry in the $m_l = \pm 2$ orbitals making up $d_{X^2-Y^2}$. Indeed, this happens. Table II shows the amplitudes of the occupation matrix eigenstate in the local coordinate system. The imbalance in the $m_l = +2$ and $m_l = -2$ occupations in the spin-up channel results in a surprisingly large (for an e_g shell) orbital moment.

VI. SUMMARY

Materials such as $KOsO_4$ with an e_g^1 configuration are expected to have a negligible orbital moment. Mixing of t_{2g} character is required, which is aided by small crystal field splitting and structural symmetry lifting. We have studied the interplay of strong correlation effects

TABLE II: Amplitude coefficients of the occupied orbital, expressed with respect to complex orbitals and both spin components, in the the local coordinate system with spin along the [100] direction.

	m_l				
	0	–1	+1	–2	2
$\vert\uparrow\rangle$	–0.47	$-0.09i$	$0.11i$	0.50	0.70
$\vert\downarrow\rangle$	$0.01i$	–0.08	0.07	$-0.07i$	$0.08i$

and large spin-orbit coupling strength, and have found that an additional characteristic is very important: the additional symmetry breaking of the electronic state by spin-orbit coupling itself. The spin-direction dependent orbital moment in this Os^{7+} e_g^1 system has been analyzed and understood. The occupied orbital without spin-orbit coupling is $d_{z^2}|\uparrow\rangle$. For spin along the [001] axis, indeed there is negligible mixing with $m_l \neq 0$ orbitals and the only change due to SOC is a few percent reduction in the spin moment.

For the spin along the in-plane [100] axis, however, SOC further breaks $x \leftrightarrow y$ symmetry, inducing a population imbalance in the $m_l = -2$ and $m_l = +2$ orbitals relative to the spin direction, which drives the unexpectedly large orbital moment $M_L = -0.2\mu_B$. This moment cancels half of the Os spin moment, and the accompanying magnetocrystalline anisotropy favors this [100] spin orientation.

VII. ACKNOWLEDGMENTS

We acknowledge J. Yamaura for communications on resistivity measurement, and J. Kuneš for useful discussions on the calculations of Wannier functions including SOC. This research was supported by National Research Foundation of Korea Grant No. NRF-2013R1A1A2A10008946 (K.W.L.) and by U.S. Department of Energy Grant No. DE-FG02-04ER46111 (W.E.P.).

* Electronic address: mckwan@korea.ac.kr
† Electronic address: pickett@physics.ucdavis.edu

[1] C. L. Kane and E. J. Mele, Phys. Rev. Lett. **95**, 146802 (2005).
[2] K.-W. Lee and W. E. Pickett, EPL **80**, 37008 (2007).
[3] O. Nganba Meetei, W. S. Cole, M. Randeria, and N. Trivedi, arXiv:1311.2823.
[4] K. W. H. Stevens, Proc. R. Soc. London, Ser. A **219**, 542 (1953).
[5] J. B. Goodenough, Phys. Rev. **171**, 466 (1968).
[6] C. Lacroix, J. Phys. C **13**, 5125 (1980).
[7] H. Jin, H. Jeong, T. Ozaki, and J. Yu, Phys. Rev. B **80**, 075112 (2009).
[8] G. Chen and L. Balents, Phys. Rev. B **84**, 094420 (2011).
[9] T. Dodds, T.-P. Choy, and Y. B. Kim, Phys. Rev. B **84**, 104439 (2011).
[10] M.-C. Jung, Y.-J. Song, K.-W. Lee, and W. E. Pickett, Phys. Rev. B **87**, 115119 (2013).
[11] H. Matsuura and K. Miyake, J. Phys. Soc. Jpn. **82**, 073703 (2013).
[12] R. Arratia-Pérez, Chem. Phys. Lett. **203**, 409 (1993).
[13] V. Pershina, T. Bastug, and B. Fricke, J. Chem. Phys. **122**, 124301 (2005).
[14] V. Pershina, J. Anton, and T. Jacob, Phys. Rev. A **78**, 032518 (2008).
[15] W. Levason, M. Tajik, and M. Webster, J. Chem. Soc., Dalton Trans., 1735 (1985).
[16] Z. Hiroi, S. Yonezawa, Y. Nagao, and J. Yamaura, Phys. Rev. B **76**, 014523 (2007).
[17] A. Koda, W. Higemoto, K. Ohishi, S. R. Saha, R. Kadono, S. Yonezawa, Y. Muraoka, and Z. Hiroi, J. Phys. Soc. Jpn. **74**, 1678 (2005).
[18] J. Yamaura (private communication).
[19] A. Zalkin and D. H. Templeton, Acta Crystallogr. **6**, 106 (1953).
[20] M. Pley and M. S. Wickleder, J. Solid State Chem. **178**, 3206 (2005).
[21] G. S. Rohrer, *Structure and Bonding in Crystalline Materials*, (Cambridge University Press, Cambridge, U.K., 2001).
[22] K. Schwarz and P. Blaha, Comput. Mater. Sci. **28**, 259 (2003).
[23] K. Koepernik and H. Eschrig, Phys. Rev. B **59**, 1743 (1999).
[24] J. Kuneš, R. Arita, P. Wissgott, A. Toschi, H. Ikeda, and K. Held, Comput. Phys. Commun. **181**, 1888 (2010).
[25] Y. Zhang, N. A. W. Holzwarth, and R. T. Williams, Phys. Rev. B **57**, 12738 (1998).
[26] G. L. Krasko, Phys. Rev. B **36**, 8565 (1987).